Free-Space Micromachined Optical Switches for Optical Networking

L. Y. Lin, *Member, IEEE,* E. L. Goldstein, *Member, IEEE,* and R. W. Tkach, *Senior Member, IEEE*

Abstract— **Fiber-optic switches with high port count have emerged as leading candidates for deployment in future optical transport networks, where restoration and provisioning in the optical layer will become increasingly important. This paper reviews the principle and performance of free-space micromachined optical switches (FS-MOS) featuring free-rotating hinged micromirrors. A single-chip FS-MOS that implements the critical function of bridging—essential for restoration in core optical networks—is also proposed and demonstrated. The scalability of FS-MOS devices, and the dependence of their insertion losses on mirror-angle, are estimated theoretically. Simulation results suggest that the FS-MOS approach holds considerable promise for being expandable to the port-count values that will be needed in future core-transport lightwave networks.**

Index Terms— **Free-space, micromachined, optical crossconnect, optical networking, optical switch, provisioning, restoration.**

I. Introduction

DUE TO VERY rapid increases in core-transport-network demand, in the bit rates of individual services, and in the number of wavelength-channels being built into WDM transport systems, fiber-optic switches with large port count have quickly emerged as perhaps the most important yet-unrealized technological need in future high-capacity lightwave networks. These network elements will be chiefly used for network restoration, to begin with, with substantial provisioning value likely emerging thereafter. Optical switching technologies offer the potential advantages of bit-rate transparency, low power consumption, small volume, and low cost. Nevertheless, the requirements in port count (on the order of 512×512 in three to five years) and loss budget represent deep challenges that have not yet been met by any current photonic switching technology. Although conventional mechanical switches can achieve high optical quality, they are large in size and mass, and are thus relatively slow in switching speed. On the other hand, guided-wave solid-state switches, though compact, generally have high loss and high cross talk. The inherent disadvantages of these technologies thus, appear to limit their expandability to the port counts mentioned above.

By contrast, micromachined free-space optical-switching technology holds particular appeal in this application because it combines the advantages of free-space interconnection—low loss and high optical quality—with those of monolithic integrated optics, namely, compactness. Various small-scale (2×2) micromachined switches [1], [2] utilizing sliding micromirrors have been demonstrated. In addition, collimating optics and rotating micromirrors have also been proposed as a means of achieving high-density optical switches [3]–[5]. Given the fertility that the field of micro-optical systems is beginning to show, and the considerable variety of switching devices that has already emerged, it is likely that diverse applications will be best suited to diverse switching technologies. However, for the application of restoration and provisioning in core-transport lightwave networks, free-space micromachined optical switches (FS-MOS) with free-rotating hinged micromirrors are particularly attractive; this is because such applications do not require frequent switching, but do require very high reliability even for switch mirrors that remain in one switching state for extended periods on the order of years. Furthermore, the submillisecond switching times exhibited by FS-MOS devices are well matched to the needs of restoration and provisioning in core-transport lightwave-communications networks.

In Section II, we will review the design and performance of FS-MOS devices. Their application to optical-network restoration will be proposed and demonstrated in Section III. In Section IV, we theoretically analyze the scalability of FS-MOS devices.

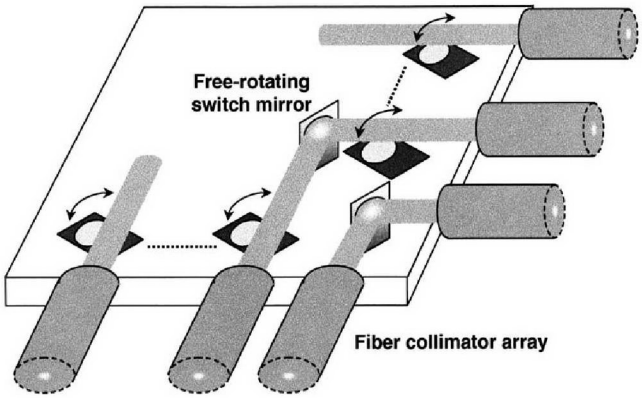

Fig. 1. Schematic drawing of the matrix free-space micromachined optical switch (FS-MOS).

II. Device Design and Performance

The working principle of a matrix FS-MOS is shown in Fig. 1. The microactuated free-rotating mirrors are monolithically integrated on a silicon chip by means of surface-micromachining fabrication techniques. The collimated light is switched to the desired output port by rotating a selected mirror. Fig. 2 contains a schematic drawing of the actuated

Manuscript received June 2, 1998; revised September 2, 1998.
The authors are with AT&T Labs-Research, Red Bank, NJ 07701 USA.
Publisher Item Identifier S 1077-260X(99)00644-9.

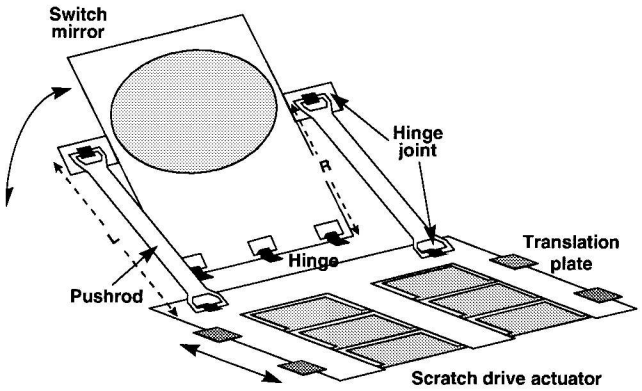

Fig. 2. Schematic drawing of the microactuated free-rotating switch mirror.

mirror. The microfabricated hinges [6] anchor the mirror on the Si substrate. The modified interleaved hinges constitute the hinge joints, through which the mirror is connected to the translation stage by push rods. The translation stage is actuated by arrays of scratch-drive actuators (SDA's) [7]. The design efficiently converts the translation of the microactuators to rotation of the mirror.

FS-MOS chips utilizing mirrors of the above-described structure have been fabricated using the MCNC MUMP's (multiuser MEMS processes) fabrication process.[1] The epitaxial layers consist of one Si_3N_4 layer for insulation; three polysilicon layers for ground-plane purposes (poly-0) and for mechanical structures (poly-1 and poly-2); two phosphosilicate glass layers for use as sacrificial material; and one gold layer for use in fabricating electrical contacts and mirror coatings. The mirror and the translation plate are built on the second polysilicon (poly-1) layer, and anchored to the substrate through hinge and guiding rail structures built on the third polysilicon layer (poly-2). The SDA's are L-shaped polysilicon plates formed on poly-2. The hinge joints consist of interleaved poly-1/poly-2 structures, and are connected to the push rods built on poly-2. After the epitaxial growth, the sacrificial material is selectively etched by immersing the device in hydrofluoric acid, thus releasing the mechanical structures from the Si substrate. Fig. 3 shows the top-view photograph of an 8×8 switch. The whole switch fabric occupies a chip area of 1×1 cm^2.

The free-rotating micromirror structures described above offer precisely the kinds of switching speeds that core-transport-network cross connects demand. Device measurements have shown submillisecond switching times when the SDA's are actuated with $\pm$100-V square wave at 500 kHz. The maximum mirror-rotation angle is defined by the dimension of the ground electrode under the translation stage. Fig. 4 shows the measured results for the switching-time response. The switching time is 500 μs for rotating the mirror from the OFF position to the ON position. To this, one must add a 200-μs delay between the application of the switching voltage and the onset of measurable optical-switching action. For the first demonstration, the mirror is rotated down by pulling the translation plate back with polysilicon springs, resulting in an

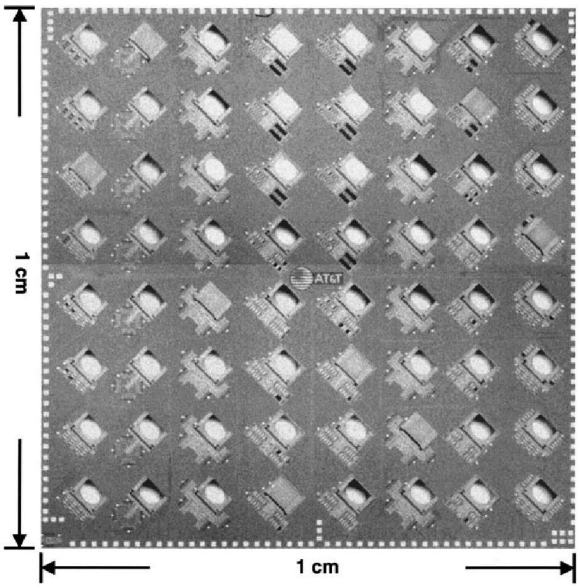

Fig. 3. Top view photograph of an 8×8 FS-MOS.

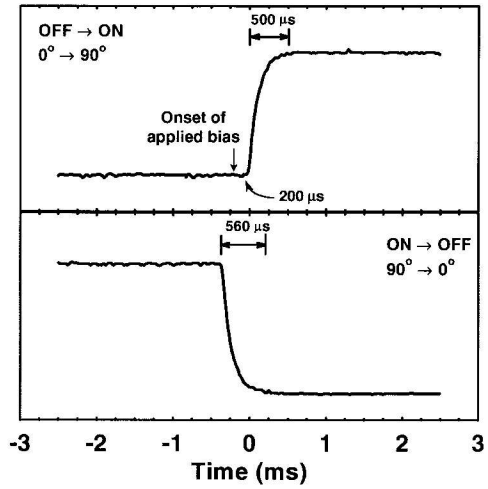

Fig. 4. Switching response of the FS-MOS.

ON $\rightarrow$ OFF switching time of 560 μs. In practical systems, the springs would likely be replaced by bidirectional SDA's. The device's switching curve shows an extinction ratio of more than 60 dB.

In the previously demonstrated 4×4 FS-MOS [4], integrated binary-amplitude Fresnel lenses were used for collimating optical beams. Binary-amplitude Fresnel lenses possess the advantage of fabrication compatibility with MUMPS. Nevertheless, they resulted in high, nonuniform insertion loss. By employing fiber collimators for input and output coupling, losses as low as 3.1–3.5 dB are achieved for the shortest and longest optical paths in an 8×8 switch, respectively. The fiber collimators consist of Grin lenses attached to single-mode fibers. The optical beam diameter at the fiber facet is 300 μm. The measurement results show slightly higher loss than the theoretical calculations in Section IV. This may be attributed to the imperfect alignment of the fiber collimators and slight curving of the mirror surfaces. The flatness of the mirror surface can be improved by depositing thinner Au (currently

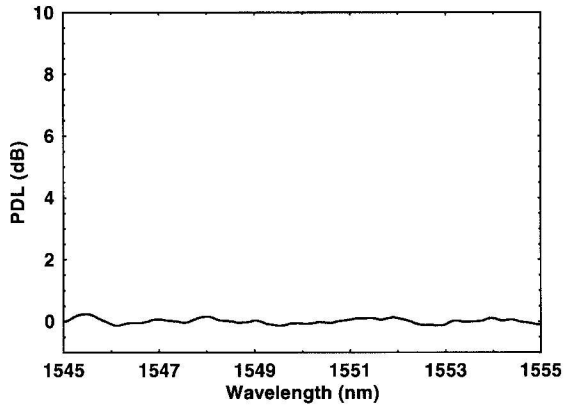

Fig. 5. Polarization-dependent loss (PDL) of FS-MOS versus wavelength. The device's PDL is below the noise floor of the measurement system.

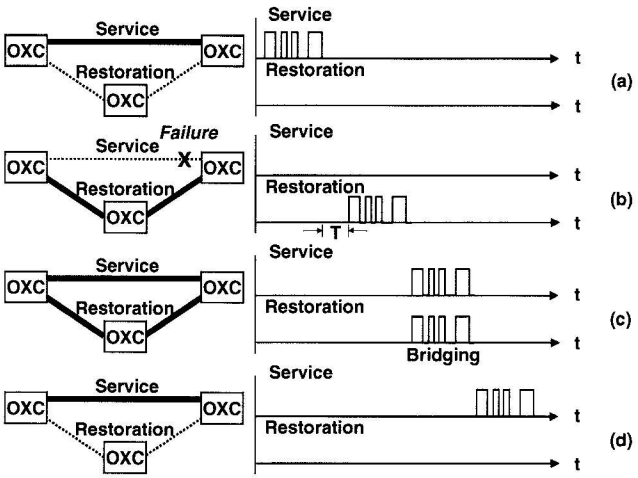

Fig. 6. Schematic illustration of the bridging operation in core-transport networks.

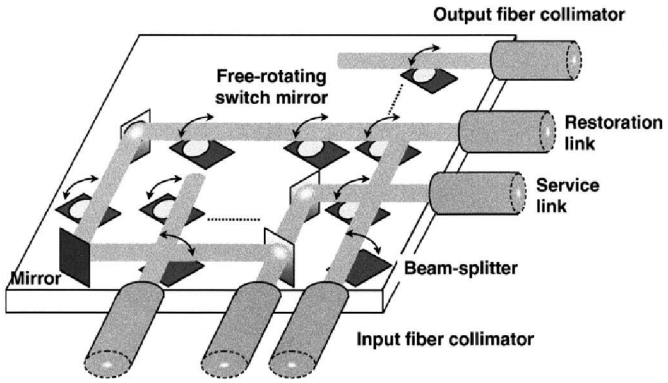

Fig. 7. Schematic of the FS-MOS incorporating the bridging function.

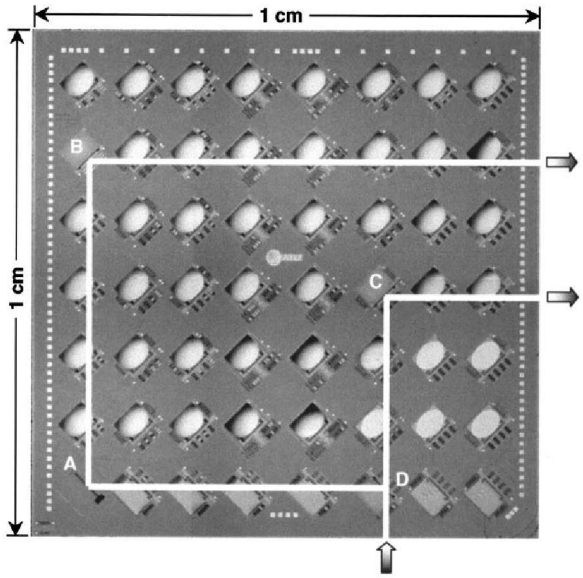

Fig. 8. Top-view photograph of the FS-MOS configured to execute bridging.

Unlike guided-wave approaches, these devices tend to exhibit very low cross talk values (< -60 dB) between adjacent channels without resorting to dilated architectures. Moreover, one substantial advantage of the FS-MOS is its low polarizations-dependent loss (PDL). Fig. 5 shows PDL as a function of the wavelength used to illuminate the switch ports. The device's PDL is seen to be smaller than the measurement system's noise floor of about 0.3 dB. In general, the very high optical qualities of these switching structures highlight the inherent virtues of free-space interconnection approaches.

III. Application in Network Restoration

Any optical switching or cross connection network element used for core-transport network restoration must provide the critical function of bridging. This is illustrated in Fig. 6. Under normal operation [Fig. 6(a)], traffic traverses the service link. Upon link failure [Fig. 6(b)], it is switched to the restoration path, sustaining an interruption of duration T. Upon repair, traffic must be *bridged* to *both* service and restoration links [Fig. 6(c)], in order to avoid a second interruption due to imperfectly synchronized head- and tail-end switching. What is critical is that the above bridging capability be incorporated erbating the already-challenging scaling demands incumbent on it.

We demonstrate here a means of accomplishing this for devices of the FS-MOS type. By integrating into the FS-MOS a few simple additional micro-optical elements, advanced functions like bridging can be incorporated at little cost in insertion loss or, ultimately, in scalability. Fig. 7 contains a schematic drawing of the FS-MOS with bridging. An additional row of beam-splitters, an additional column of free-rotating mirrors, and a fixed mirror are incorporated into the switch fabric to achieve the any-one-to-any-two bridging function. To accommodate multiple simultaneous bridging operations, multiple copies of these elements could be integrated on a substrate. The beam-splitters are fabricated using the same process as the switch mirrors, except that they consist of a 1.5-μm polysilicon plate without any reflective gold coating.

The device's operation is most readily apparent from Fig. 8. This is a top-view photograph of the FS-MOS, with array elements configured to execute bridging. The corner mirror (A) has been assembled and is held perpendicular to the substrate by spring latches [6] and precision side-latches [8]. Switch

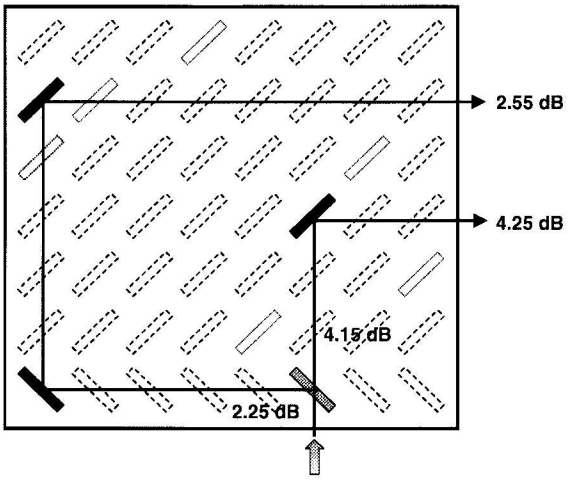

Fig. 9. Measured loss at 1.55 μm through the beam-splitter and mirrors of the FS-MOS.

up, perpendicular to the substrate. During normal operation, only switch mirror C is rotated up, providing a light path from the input to the output service link. Upon service-link failure, B and D rotate up, thus directing traffic to the restoration link. With C upright as well, traffic is bridged onto both service and restoration links. Finally, to carry out recovery, B and D are lowered, with C left upright, so that traffic again flows on the service link only.

Among the chief determinants of scalability in these devices is loss. Here, the effect upon loss of the bridging structure is characterized. The insertion losses through beam-splitters and mirrors, for both service and restoration paths, are measured by coupling light at 1550 nm into the switch fabric using a fiber collimator. Losses along the optical paths were then measured with a large-area detector. Fig. 9 shows the results. Insertion losses along the beam-splitter's transmission and reflection paths were 4.15 and 2.25 dB, respectively. The service path's switch mirror adds an additional 0.1-dB loss. Along the restoration path, the loss from beam-splitter to output is 0.3 dB. The total excess loss for the two paths is 0.31 dB, of which 0.09 dB results from scattering and absorption in the beam-splitter itself.

IV. Scalability Analysis

In this section, we analyze loss versus port count expected for FS-MOS-type devices, emphasizing the dependence of loss on optical beam size. We also analyze the dependence of loss on imperfect angular alignment in the switch mirrors and describe means of optimizing fiber-coupling efficiency. Gaussian-beam approaches are employed [9]. The analysis and simulation results described here are generally applicable not only to the FS-MOS, but also to optical matrix switches with free-space beam propagation. The detailed theoretical algorithm will be reported elsewhere.

First, we assume that the optical beam that emerges from the input fiber has a minimum Gaussian-beam waist at the point of emergence. We characterize this by the $1/e$ half-beam-width w_0 at the facet of the input fiber. Due to its significance, it

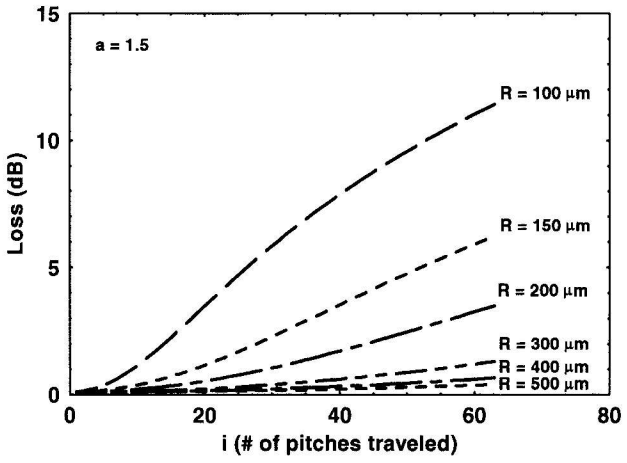

(a)

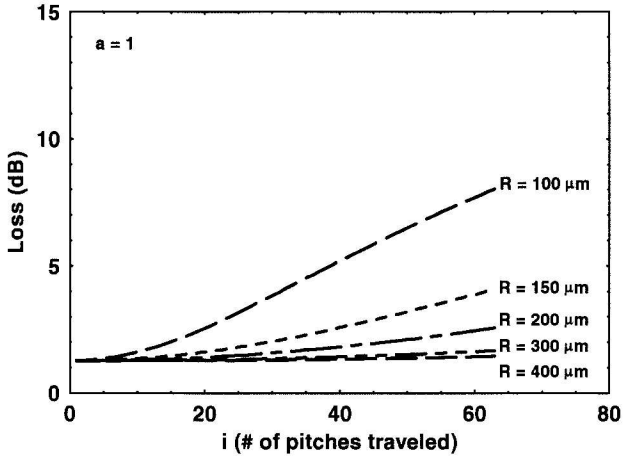

(b)

Fig. 10. Loss versus number of pitches traveled for various mirror radii, assuming (a) $a = 1.5$, (b) $a = 1$, where a is the ratio of mirror radius to Gaussian beam waist.

switch-mirror radius R divided by the beam waist w_0. Thus, the dimensionless quantity $R/w_0 = a$, is a variable that can be optimized depending on the value of R.

The coupling efficiency through the FS-MOS is obtained by calculating the overlap integral of the wave functions of the optical beam and the fiber mode at the receiving fiber facet. The optical beam diverges as it propagates through free space due to the finite beam waist, thus limiting the coupling efficiency. It is clear that the optimal size of the Gaussian beam will represent a compromise between competing forces. Although Gaussian beams with larger beam diameters exhibit smaller divergence angles, the mirror size that would be required increases with beam diameter. As a result, the propagation distance of the optical beam also increases for a given device port-count. In particular, the pitch p between adjacent mirrors is geometrically related to the mirror radius R by $p = 3R + 800$ (in μm) for the FS-MOS design described here. Fig. 10(a) shows the simulation results for various mirror radii and beam sizes, assuming that $a = 1.5$, i.e., that the mirror is 1.5 times as large as the beam waist. The variable i labeling the abscissa in Fig. 10 represents the total propagation

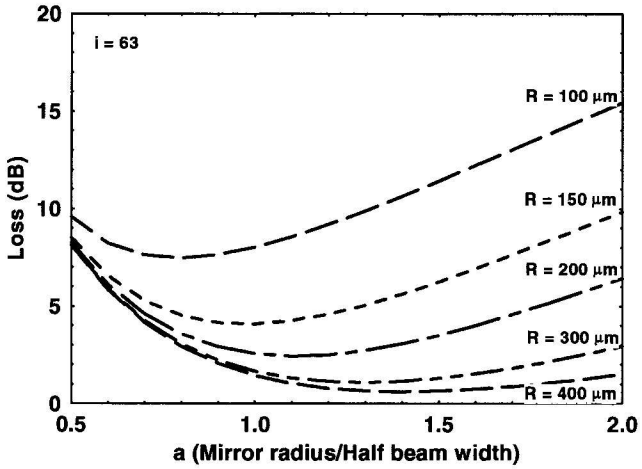

(a)

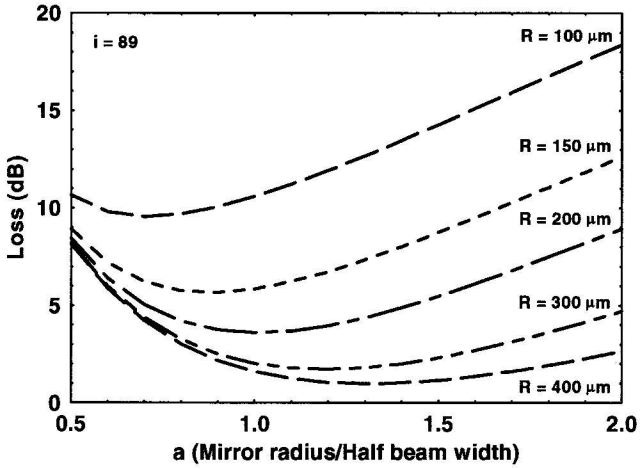

(b)

Fig. 11. Highest loss in a (a) 32×32 and (b) 45×45 switch fabric versus a for various mirror radii.

in number of mirror pitches or, roughly, rows plus columns. The distance between the input/output fiber facet and the closest mirror is assumed to be $p/2$. Therefore, $i = 63$ is the number of pitches corresponding to the longest path in a 32×32 switch. The coupling loss in Fig. 10 is seen to decrease rapidly as the mirror/beam size increases, suggesting that beam divergence is the dominating factor in this region. Nevertheless, the effect saturates as the mirror radius increases beyond 400 μm.

While keeping the mirror radius R unchanged, the Gaussian-beam waist w_0 can be increased to reduce the divergence effect. The crosstalk induced by scattering of the optical beam from the mirror edge is expected to be negligible in most cases where separation between adjacent mirrors is sufficient. Fig. 10(b) shows the simulation results for $a = 1$, that is, for mirror radius equal to beam waist. Compared to Fig. 10(a), the loss is greatly reduced for small mirrors. As the optical beam cannot be captured completely by the reflecting mirror when it arrives at the mirror surface due to beam divergence, a loss floor of $\sim$1.3 dB appears in the results.

This suggests the existence of an optimal value of a,

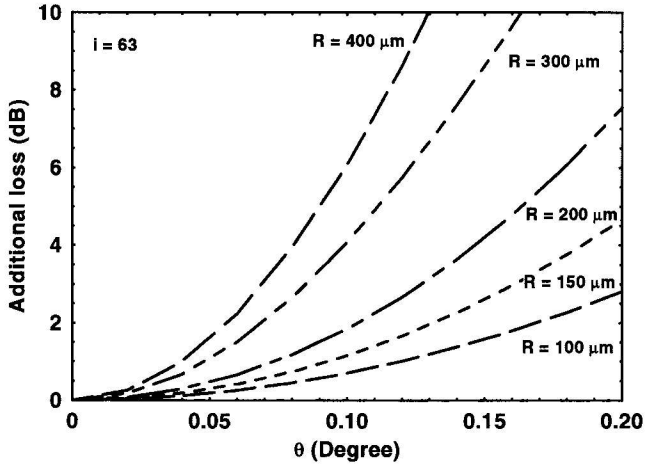

Fig. 12. Additional loss due to mirror-angle variation for the longest path in a 32×32 switch fabric. λ is twice the mirror-angle variation. The values of a have been optimized for different mirror radii.

Fig. 11(a) and (b) is calculated for the cases of $i = 63$ and 89, that is, for the longest optical paths and, therefore, highest losses in a 32×32 and 45×45 switch, respectively. The value of the optimal a increases as the mirror radius increases. This is because the effect of optical-beam divergence is more significant for small beam sizes.

The minimum loss for the longest optical path through a 512×512 or 1024×1024 switch fabric can, therefore, be obtained by simulation. We assume for illustration the use of three-stage Clos switch-fabric architecture [10] as a means of constructing large-port-count switches using smaller constituent switch modules. Assuming the input port count of each switch module in the first stage is n, in order to achieve the property of strict nonblocking, the output port count of the switch module needs to be greater than $2n - 1$. This is also the required input and output port count for the switch module in the second stage. The switch module in the third stage is a mirror image of that in the first stage. Therefore, to construct a 512×512 switch fabric, one can employ 32 layers, with 16×32, 32×32, and 32×16 switch modules comprising the three stages. For a 1024×1024 switch fabric, 45 layers of 23×45, 45×45, and 45×23 switch modules may be used. With these assumptions, using the approach described above, it can be shown that a mirror radius of 200 μm achieves a 5.8 dB loss through the longest path of a 512×512 switch fabric. Similarly, a mirror radius of 250 μm achieves 5.8-dB loss through the longest path of a 1024×1024 switch fabric. In each of these cases, the switch's second stage imposes loss values indicated in Fig. 11; the first and third stages impose smaller losses due to their smaller size.

The results described above assume a perfectly aligned optical system. To characterize imperfectly aligned systems, the dependence of coupling efficiency on the angular error in mirror alignment may be captured by performing a coordinate-system transformation on the wave function of the propagating Gaussian beam. Fig. 12 shows the additional loss versus twice the mirror-angle variation for various mirror radii, assuming the traversed number of pitches is fixed at $i = 63$. The value

DOCKET ALARM

Explore Litigation Insights

Docket Alarm provides insights to develop a more informed litigation strategy and the peace of mind of knowing you're on top of things.

Real-Time Litigation Alerts

Keep your litigation team up-to-date with **real-time alerts** and advanced team management tools built for the enterprise, all while greatly reducing PACER spend.

Our comprehensive service means we can handle Federal, State, and Administrative courts across the country.

Advanced Docket Research

With over 230 million records, Docket Alarm's cloud-native docket research platform finds what other services can't. Coverage includes Federal, State, plus PTAB, TTAB, ITC and NLRB decisions, all in one place.

Identify arguments that have been successful in the past with full text, pinpoint searching. Link to case law cited within any court document via Fastcase.

Analytics At Your Fingertips

Learn what happened the last time a particular judge, opposing counsel or company faced cases similar to yours.

Advanced out-of-the-box PTAB and TTAB analytics are always at your fingertips.

API

Docket Alarm offers a powerful API (application programming interface) to developers that want to integrate case filings into their apps.

LAW FIRMS
Build custom dashboards for your attorneys and clients with live data direct from the court.

Automate many repetitive legal tasks like conflict checks, document management, and marketing.

FINANCIAL INSTITUTIONS
Litigation and bankruptcy checks for companies and debtors.

E-DISCOVERY AND LEGAL VENDORS
Sync your system to PACER to automate legal marketing.